Nano Energy 137 (2025) 110811

Contents lists available at ScienceDirect

Nano Energy

journal homepage: www.elsevier.com/locate/nanoen

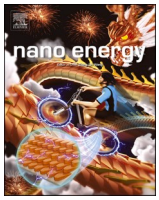

Decoding systematic effects and mass transport in H_2O_2 production via Au_x/C ORR electrocatalysis

Ji Sik Choi [a,b,**], Guilherme V. Fortunato [b,c,**], Marko Malinovic [a,b], Ezra S. Koh [a,b], Raquel Aymerich-Armengol [d], Christina Scheu [d], Huize Wang [e], Andreas Hutzler [e], Jan P. Hofmann [f], Marcos R.V. Lanza [c], Marc Ledendecker [b,e,**]

[a] Department of Technical Chemistry, Technical University of Darmstadt, Peter-Grünberg-Straße 8, Darmstadt 64287, Germany
[b] Sustainable Energy Materials, Technical University Munich, Campus Straubing, Schulgasse 22, Straubing 94315, Germany
[c] São Carlos Institute of Chemistry, University of São Paulo, Avenida Trabalhador São-Carlense 400, São Carlos, SP 13566-590, Brazil
[d] Nanoanalytics and Interfaces, Max-Planck-Institute for Sustainable Materials GmbH, Max-Planck-Straße 1, Düsseldorf 40237, Germany
[e] Forschungszentrum Jülich GmbH, Helmholtz-Institute Erlangen-Nürnberg for Renewable Energy (IET-2), Cauerstraße 1, Erlangen 91058, Germany
[f] Surface Science Laboratory, Department of Materials, and Geosciences, Technical University of Darmstadt, Peter-Grünberg-Straße 4, Darmstadt 64287, Germany

ARTICLE INFO

Keywords:
Oxygen-reduction
Hydrogen peroxide production
Selectivity
Size effects
Systematic parameters

ABSTRACT

Traditionally, evaluating a catalyst's activity has focused on its intrinsic properties. However, the observed catalytic behavior can be significantly influenced by both systematic parameters and mesoscopic mass transport limitations. Although the independent roles of various factors are known, their intricate interplay within electrocatalysis remains elusive. This work presents a comprehensive investigation into the interplay between these factors in the selective generation of hydrogen peroxide (H_2O_2) via the oxygen reduction reaction (ORR) using Au_x/C catalysts with varying particle sizes. By considering the exchange of surface-bound reaction intermediates between the electrode and bulk electrolyte, we reveal how the catalyst's surface area can influence selectivity through kinetic competition. This effect becomes particularly relevant for technologically important reactions such as the ORR, where multiple product pathways exist. This study underscores the need for a multi-scale approach that considers all these factors, especially for reactions involving multiple reaction pathways. Precise tuning of these parameters is essential for achieving a reliable and equitable assessment of electrocatalysts, paving the way for optimizing H_2O_2 production and similar multi-step electrocatalytic reactions.

1. Introduction

H_2O_2 has been listed as a key chemical component in the development of a more sustainable society, with remarkable growth in its production. In 2022, the global demand for H_2O_2 reached approximately 4.4 million tonnes, and forecasts predict a rise at a 5.9 % compound annual growth rate until 2032 [1,2]. One promising path for the production of H_2O_2 is the decentralized electrochemical production without the use or handling of molecular hydrogen by a selective 2-electron oxygen reduction reaction ($2e^-$ORR) [3]. Here, catalysts that reduce oxygen to H_2O_2 are needed. Traditionally, optimizing electrocatalysts for H_2O_2 production has focused on their intrinsic activity—an attribute that denotes the inherent catalytic efficiency and selectivity of the material in driving the two-electron oxygen reduction reaction. However, recent research suggests that observed catalytic behavior can be significantly influenced by factors beyond simply the intrinsic properties of the catalyst [4].

One key consideration is the role of systematic parameters. These parameters, such as interparticle distance and catalyst layer thickness, can significantly affect the local environment around the active sites and consequently influence the reaction pathway [5–7]. Additionally, mass transport limitations, which dictate the exchange of surface-bound reaction intermediates between the electrode and the bulk electrolyte, can play a crucial role in selectivity [8]. By influencing the availability of reactants and intermediates at the active sites, mass transport limitations can introduce kinetic competition, particularly for reactions like ORR with multiple possible product pathways (e.g., H_2O_2 vs·H_2O). While the impact of intrinsic activity has been extensively studied, a comprehensive understanding that considers the interplay between intrinsic properties, systematic parameters, and mass transport

** Corresponding authors at: Sustainable Energy Materials, Technical University Munich, Campus Straubing, Schulgasse 22, Straubing 94315, Germany.
E-mail addresses: jisik.choi@tum.de (J.S. Choi), g.fortunato@tum.de (G.V. Fortunato), marc.ledendecker@tum.de (M. Ledendecker).

https://doi.org/10.1016/j.nanoen.2025.110811
Received 22 October 2024; Received in revised form 23 January 2025; Accepted 21 February 2025
Available online 23 February 2025

limitations remains elusive. Despite individual optimization efforts on the particle size [9–16], interparticle distance [13,17–21], and catalyst layer thickness [22–25] for the ORR, the collective influence on H_2O_2 activity and selectivity is still not fully understood. This lack of a multi-scale approach can lead to misinterpretations of the observed catalytic behavior and hinder the development of truly optimized electrocatalysts for H_2O_2 production.

This work addresses this gap in knowledge by investigating the combined influence of these factors on H_2O_2 production via ORR electrocatalysis. We employ Au_x/C catalysts with varying particle sizes as a model system to explore the interplay between intrinsic activity, systematic parameters, and mass transport limitations. By utilizing a rotating ring-disk electrode (RRDE) setup for rapid catalyst screening, we systematically elucidate the specific effects of each factor on H_2O_2 selectivity. This multi-scale approach provides a deeper understanding of the complex interplay governing H_2O_2 production and paves the way for the design of highly efficient electrocatalysts.

2. Results and discussion

2.1. Catalyst characterization

To evaluate the effect of particle size on the ORR, gold nanoparticles (Au NPs) with sizes of approximately 3, 4, 10, and 16 nm were utilized.

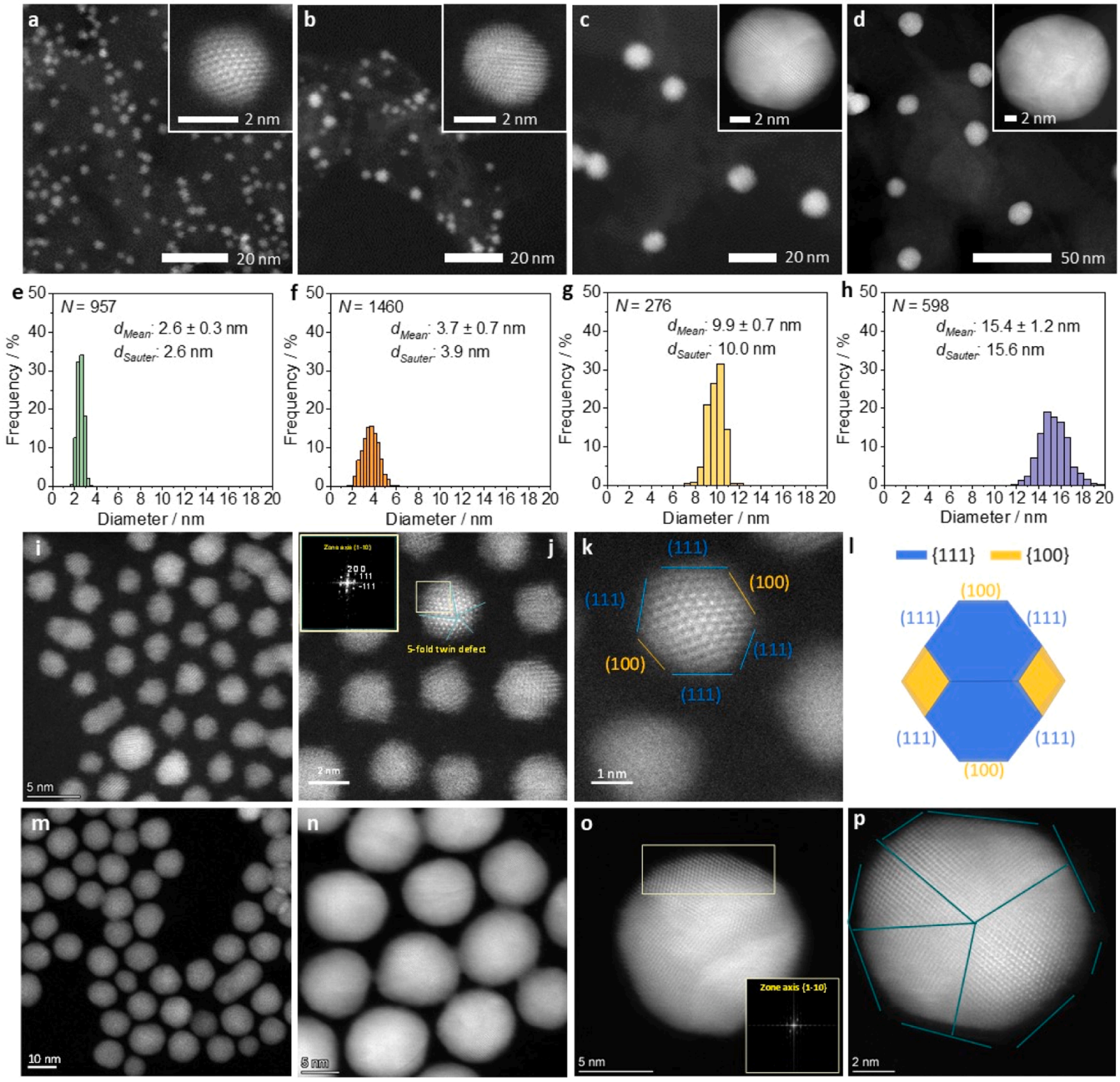

Fig. 1. (a-d) STEM images of 20 wt% Au_x/C catalysts and (e-h) respective particle size distribution with varying particle sizes: 3 (a, e), 4 (b, f), 10 (c, g), and 16 nm (d, h). Insets show HAADF-(HR)STEM images of the corresponding unsupported Au NPs. *N*, d_{Mean}, and d_{Sauter} stand for the number of analyzed Au NPs, the mean number diameter, and the Sauter diameter, respectively. Further HAADF-(HR)STEM images of 3 nm (i-k) and 10 nm (m-p) Au nanoparticles are shown, along with the corresponding facet assignments. Insets present fast Fourier transform (FFT) images for the {1−10} zone axis of the highlighted areas. (l) A schematic representation of single-crystal nanoparticle is provided, showcasing predominantly (111) and (100) facets.

The unsupported Au NPs possess spherical character, as illustrated in the insets of Fig. 1a-d, characterized using high-angle annular dark field (high resolution) scanning transmission electron microscopy (HAADF-(HR)STEM). A detailed description of the parameters used is provided in the supporting information. Subsequently, the nanoparticles were homogeneously supported on Printex XE2B (C), which has a BET surface area of 1000 $m^2\ g^{-1}$ [26], and evaluated through scanning transmission electron microscopy (STEM) investigations, as demonstrated in Fig. 1a-d. Statistical characterization of such 20 wt% Au_x/C samples revealed average nanoparticle sizes of 3 (2.6 ± 0.3 nm, Au_3/C), 4 (3.7 ± 0.7 nm, Au_4/C), 10 (9.9 ± 0.7 nm, Au_{10}/C), and 16 (15.4 ± 1.2 nm, Au_{16}/C), as illustrated in Fig. 1e-h. These values are utilized for calculating interparticle distances of Au NPs. Conversely, the Sauter diameter—also known as the surface area mean diameter—was used to compare the specific surface area obtained by the electron microscopy measurements with the electrochemically active surface area (ECSA) of the Au NPs. This approach provides a more accurate representation of the overall surface area of the Au NPs, as detailed in the particle size histograms of Fig. 1e-h. The mean number diameter (d_{Mean}), Sauter diameter (d_{Sauter}), and specific surface area of the Au NPs were calculated for each sample by counting individual particles and applying Eqs. 1, 2, and 3, respectively.

$$d_{Mean} = \frac{\sum d_i}{N} \tag{1}$$

$$d_{Sauter} = \frac{\sum d_i^3}{\sum d_i^2} \tag{2}$$

$$Specific\ surface\ area = \frac{6}{\rho_{Au} \times d_{Sauter}} \tag{3}$$

Where d_i, N, and ρ_{Au} are the diameters of the individual particles, the number of the particles, and the density of gold (19.3 g cm^{-3}), respectively.

To further examine the size-dependent morphological and structural characteristics between the samples, Fig. 1i-p presents a series of atomic-resolution HAADF-STEM images of unsupported Au nanoparticles with diameters of 10 and 3 nm. The images reveal local ordering consistent with face-centered cubic (fcc) packing of Au atoms, exhibiting characteristic lattice fringes corresponding to (111) and (100) crystal planes. Analysis of the nanoparticles indicates that while the 3 nm nanoparticles show a mixture of single-crystalline morphologies and some twinned particles, multiple grain boundaries are prevalent in the larger 10 nm particles. This observation is consistent with a recent study [27]. Close examination of the particles reveals a clear trend: as the particle diameter decreases from 10 to 3 nm, the dimensions of fcc (100) and fcc (111) facets diminish. This observation implies that in 3 nm particles, a significantly larger fraction of atoms occupy surface or near-surface positions, resulting in lower coordination numbers compared to bulk atoms [28]. Under-coordinated or unsaturated surface atoms typically exhibit enhanced reactivity, which is directly related to the superior ORR activity observed in 3 nm Au nanoparticles, as compared to their larger counterparts, as discussed in the following section.

To investigate the Au binding energies in differently sized NPs, we compared high-resolution X-ray photoelectron spectroscopy (XPS) data of Au 4 f in Fig. 2. After peak deconvolution, the Au 4 f core level spectra revealed the spin-orbit splitting components of the Au 4 $f_{7/2}$ and Au 4 $f_{5/2}$ doublets. Utilizing Au NPs of 40 nm of size as a reference, which is expected to exhibit catalytic properties closer to a bulk gold surface, we found that its 4 $f_{7/2}$ binding energy at 83.7 eV closely matches the established 84.0 eV peak of bulk Au, with a characteristic 3.7 eV separation from the 4 $f_{5/2}$ peak. As the particle size decreases from 10 to 3 nm, the binding energy increases from 84.2 to 84.5 eV. This finding aligns with the general observation that smaller particle sizes result in higher binding energies [29,30]. Additionally, the major peaks for Au^0

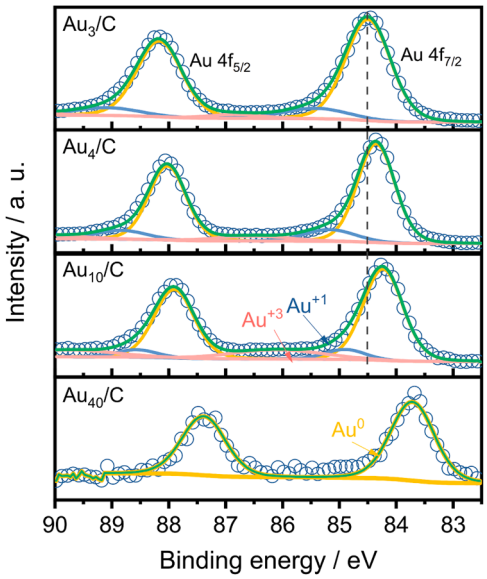

Fig. 2. High-resolution XPS spectra of the Au 4 f region for Au_x/C catalysts (x = 3, 4, and 10) and 40 nm Au NPs as a reference for bulk Au.

in Au_x/C (x = 3, 4, and 10) featured minor peaks of $Au^{\delta+}$ ($0 < \delta < 3$), suggesting the presence of undercoordinated sites [31].

2.2. Impact of particle size effect on selectivity for H_2O_2

To better understand the correlation between the particle size of the Au NPs supported on carbon and their electrocatalytic activity, we performed thin-film rotating ring-disk electrode (RRDE) measurements. These experiments were carried out in an O_2-saturated 0.1 M $HClO_4$ electrolyte, and the corresponding electrochemical data are shown in Fig. 3.

Fig. 3a presents the ORR polarization curves for 20 wt% Au_x/C catalysts with varying sizes and a carbon reference catalyst. The currents were normalized to the geometric area of the glassy carbon disk or platinum ring electrode. The carbon support, utilized as a blank test, exhibited significant overpotentials of 0.35 V_{RHE}. The averaged selectivity was calculated to be 83.6 %, based on measurements taken across a potential range from 0.5 to 0.1 V_{RHE} using Equation S2. In comparison, Au NPs supported on carbon showed a particle size dependency in the maximum current density, specific activity (SA), and ORR onset potential. The SA is determined by normalizing the mass activity to the ECSA, which itself is calculated from stable cyclic voltammograms by integrating the charge under the oxide reduction peak using a charge density of 386 $\mu C\ cm_{Au}^{-2}$ for the reduction of an oxide monolayer [32]. Experimental measurements of ECSA and specific surface area calculations based on STEM data show considerable differences as Au NP size decreases (Figure S2), potentially due to occlusion by the high surface area carbon support [33–35]. As Au_x/C particle size decreases from 16 nm to 4 nm, the undercoordination of Au atoms increases, leading to a greater presence of surface steps, corner, and edge atoms on the Au surface. An increase in the surface fraction of these sites are expected to strengthen the adsorption of oxygenated species, such as O_2, *O, *OOH, and OH, thereby influencing ORR activity [14,16,36–39]. Therefore, as the Au NP size decreases, the measured ECSA varies significantly, from approximately 8 to 45 $m^2\ g_{Au}^{-1}$ (Figure S2), this resulted in a 76 % decrease in SA at 0.5 V_{RHE}, as shown in Fig. 3b. Further reducing the particle size to 3 nm, a clear size dependency in ORR activity is evident, with onset potentials shifting from 0.55 V_{RHE} for 16 nm particles to 0.67 V_{RHE} for 3 nm particles, as shown in Fig. 3a. This intrinsic particle size effects on SA and ORR onset potentials are related to shifts in the reduction potential of Au oxide species (c.f. Fig. 3c). As particle size

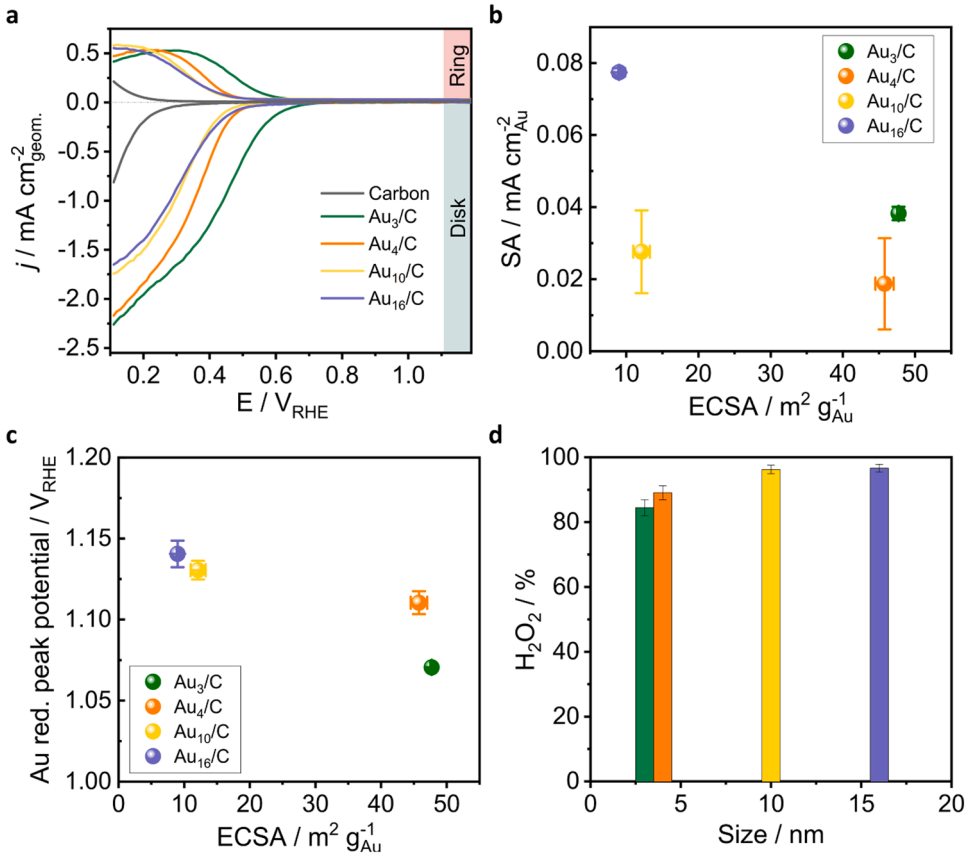

Fig. 3. ORR performance of Au_x/C catalysts with a metal loading of 20 wt%. (a) RRDE voltammograms obtained in an O_2-saturated 0.1 M $HClO_4$ electrolyte with a scan rate of 10 mV s^{-1} at 900 rpm (only the cathodic scan is shown), together with the detected H_2O_2 current on the ring at a fixed potential of 1.4 V_{RHE}. The Au loading on the electrode was fixed at 10 μg cm^{-2}. (b) Specific activity (SA) at 0.5 V_{RHE} for Au_x/C (x = 4, 10, and 16) and 0.6 V_{RHE} for Au_3/C. (c) Au-oxide reduction peak potential recorded in a N_2-saturated 0.1 M $HClO_4$ electrolyte by sweeping the potential between −0.1 and 1.7 V_{RHE} at a scan rate of 100 mV s^{-1}. (d) Averaged H_2O_2 selectivity from 0.5 to 0.1 V_{RHE} for Au_x/C (x = 4, 10, and 16) and 0.6–0.1 V_{RHE} for Au_3/C. Error bars denote 95 % confidence intervals from at least two independent measurements.

increases, there is a corresponding positive shift in Au reduction peaks, indicating easier reduction of surface oxides on larger Au particles [14,40]. Conversely, smaller particles, with their stronger Au-O bonds indicated by lower reduction potentials, possess abundant low-coordination sites such as flaws, kinks, steps, or edges that strongly bind oxygen and oxygenated species [15,41]. This enhanced adsorption on smaller particles positively influences ORR catalytic activity. Enhanced activity in smaller Au NPs is also attributed to size-related changes; theoretical calculations suggest a narrowing of d-bands, a shift closer to the Fermi level, and stronger O_2 adsorption [15,42,43]. This modification results in a marked preference for reducing O_2 to water over H_2O_2, starkly contrasting with bulk Au, which generally exhibits high H_2O_2 selectivity due to lower *OOH binding energies [43]. Previous adsorption studies on single-crystal Au electrodes and DFT analyses have revealed the structural characteristics of Au surfaces strongly influence ORR activity and selectivity [16,28,44–55]. Specifically, Au(100) facets and low-coordination sites (e.g., edges and corners) exhibit higher catalytic activity and preferentially follow the 4-electron pathway to water, while Au(111) facets tend toward the $2e^-$ pathway, mainly in alkaline conditions. Smaller Au NPs, with a higher proportion of these low-coordination sites, mimic the behavior of Au(100) facets, enhancing ORR activity and water selectivity. A detailed discussion of these structure- and size-dependent effects is provided in the Supporting Information. Fig. 3d illustrates this effect, showing a decline in H_2O_2 selectivity from 96.7 % for 16 nm NPs to 84.5 % for 3 nm Au NPs, under consistent experimental conditions: 20 wt% Au on carbon supports and 10 $\mu g\ cm^{-2}$ Au on the disk electrode, ensuring uniform catalyst layer thickness.

As particle size increases in catalysts with constant metal loading, the distance between particles (interparticle distance) changes. This directly impacts overall performance. Inaba *et al.* reported a decrease in oxophilicity when decreasing the interparticle distance influencing the overall binding affinity of oxygen intermediates on Pt [19]. However, accurately measuring interparticle spacing in a 3D catalytic system presents challenges due to the inherent randomness and uncertainty. Moreover, techniques like TEM project 3D structures onto a 2D plane, making it less effective for determining interparticle distance in such systems [56]. To address these challenges and ensure consistent comparisons with previous literature on metal-carbon composites [17,21,57], we calculated the edge-to-edge interparticle distance using Eq. 4 assuming a homogeneous distribution:

$$d_{ip} = \sqrt{A/N} - d_{Mean} \tag{4}$$

Where d_{ip}, A, N, and d_{Mean} are the interparticle distance, BET surface area of the carbon support (for Printex XE2B was used 1000 $m^2\ g^{-1}$), number of Au NPs, and mean number diameter of Au NPs, respectively. The concentration of Au nanoparticles (NPs) is as follows: 2.21×10^{14} NPs/mL for 3 nm, 4.37×10^{13} NPs/mL for 4 nm, 4.96×10^{12} NPs/mL for 10 nm, and 6.20×10^{11} NPs/mL for 16 nm. The calculated interparticle distances are 30, 66, 191, and 548 nm for 3, 4, 10, and 16 nm Au/C, respectively. The notably shorter interparticle distance for the 3 nm NPs could contribute to the decline in selectivity in conjunction with NP size. This observation motivates further investigation into how the compact interparticle distance between smaller NPs, and potentially

other systematic factors, influence selectivity, a topic explored in the subsequent section.

2.3. Impact of interparticle spacing on selectivity for catalysts

Fig. 4a presents a schematic that illustrates the influence of interparticle distance on H_2O_2 selectivity. To experimentally manipulate this distance, we utilized a colloidal suspension of Au NPs, varying the Au to carbon ratios. This approach allowed us precise control over the spacing between nanoparticles, effectively avoiding particle agglomeration. Among the various catalysts tested, the Au_3/C catalyst was selected for deeper exploration owing to its unique ability to generate both H_2O_2 and H_2O. The catalytic activity of the ORR for the Au_3/C catalyst, with variations in interparticle distances, is depicted in Fig. 4b. Each color represents a different Au loading on the electrode, i.e., 5, 10, and 20 $\mu g\ cm^{-2}$ at a certain interparticle distance. Fig. 4b demonstrates a slight decrease in the SA value with increasing interparticle distance, considering the small shift of ORR onset potential (c.f. full LSV curves provided in Figure S3). On the other hand, as seen in Fig. 4c, an increase in interparticle distance led to notable variations in H_2O_2 selectivity, correlating with the amounts of Au on the electrode.

The relationship between interparticle distance and H_2O_2 selectivity revealed that expanding the interparticle space from 30 to 60 nm between Au NPs in the Au_3/C catalyst significantly boosted H_2O_2 selectivity. This enhancement was more pronounced with greater Au loadings on the electrode. Specifically, a 2 % increase in selectivity was noted with a loading of 5 μg of Au per unit area of the electrode, and this effect was more significant with larger amounts of Au, resulting in selectivity improvements of 8 % and 16 % at Au loadings of 10 and 20 $\mu g\ cm^{-2}$, respectively. By contrast, when the interparticle distance was altered from 30 to 47 nm, a minor decrease in selectivity, by 2 % and 1 % for Au loadings of 10 and 20 $\mu g\ cm^{-2}$, respectively, was observed. This indicates an interplay between the interparticle distance and the catalyst layer thickness, both of which significantly influence the catalytic performance by altering intermediate diffusion and the probability of re-adsorption.

As the interparticle distance was adjusted by varying the Au to carbon ratio, maintaining a consistent catalyst layer thickness proved challenging. For instance, widening the interparticle gap to 47 nm thickened catalyst layer significantly impacts mass transport dynamics. This alteration results in increased trapping of produced H_2O_2 within the pores of the catalyst layer, heightening the probability of re-adsorption and continued reduction. The closer proximity of Au NPs in the surrounding area further facilitates this process, promoting the subsequent reduction of H_2O_2 to H_2O and, consequently, reducing H_2O_2 selectivity. These phenomena are particularly evident at lower interparticle distances (30 and 47 nm) and higher catalyst loadings (10 and 20 $\mu g\ cm^{-2}$). However, at an interparticle distance of 60 nm, the influence of interparticle distance became more dominant over the effects of layer thickness. This is supported by the observed minor selectivity variation of 6 % at this interparticle distance changing the Au amounts.

However, many studies for energy conversion reactions such as 4e⁻ORR, the cathode reaction in a fuel cell, that regulate interparticle distance by adjusting the metal-to-carbon support ratio often overlook the catalyst layer thickness, which inevitably accompanies the control of interparticle distance [19,20,56,58]. When intermediates such as H_2O_2 are the desired final products, as in the case of the ORR, this factor becomes critical and must not be overlooked. Regarding this issue, a more detailed discussion is provided in the following section. Here, the estimated catalyst layer thickness ranges from 90 nm to 1.53 μm, depending on the interparticle distance and Au loading, which complicates the analysis of the interparticle distance effects, as mentioned earlier. To isolate the impact of interparticle distance, we focused on samples with consistent catalyst layer thicknesses (380–470 nm), effectively minimizing the influence of variables such as particle size and layer thickness (Figs. 5b and 5c). With ECSA values held constant (Fig. 5b), a minor decrease in specific activity was observed, while selectivity for H_2O_2 surged from 76 % to 93 % as the interparticle distance increased from 30 to 65 nm. Our group's previous studies demonstrated that interparticle distance critically influences H_2O_2 selectivity by modulating re-adsorption dynamics [21,59]. Building on these findings, our current experimental results (Fig. 5 and S3) further confirm this relationship, indicating that reduced interparticle distance and thicker catalyst films enhance H_2O_2 re-adsorption and its subsequent reduction. Mechanistically, computational and *in situ* spectroscopic studies confirm that the *OOH intermediate plays a central role in ORR on Au surfaces [52–54, 60–62]. The adsorption of *OOH and its subsequent protonation to form H_2O_2 are energetically favorable on Au surfaces, especially on Au(111), where the moderate binding energy prevents O–O bond scission and enhances selectivity toward H_2O_2. Electrochemical data further suggest that at potentials more negative than the potential of zero charge (PZC, ~0.5 V_{RHE}), electrostatic repulsion suppresses HO_2^- adsorption, limiting further reduction of H_2O_2 [46,50,63]. This mechanism supports the hypothesis that H_2O_2 selectivity decreases at lower interparticle distance due to enhanced re-adsorption and further reduction. At lower interparticle distance and with thicker catalytic films, the decline in H_2O_2 selectivity is more prominent, suggesting that H_2O_2 production dominates under these conditions. Higher overpotentials (<0.4 V_{RHE}, c.

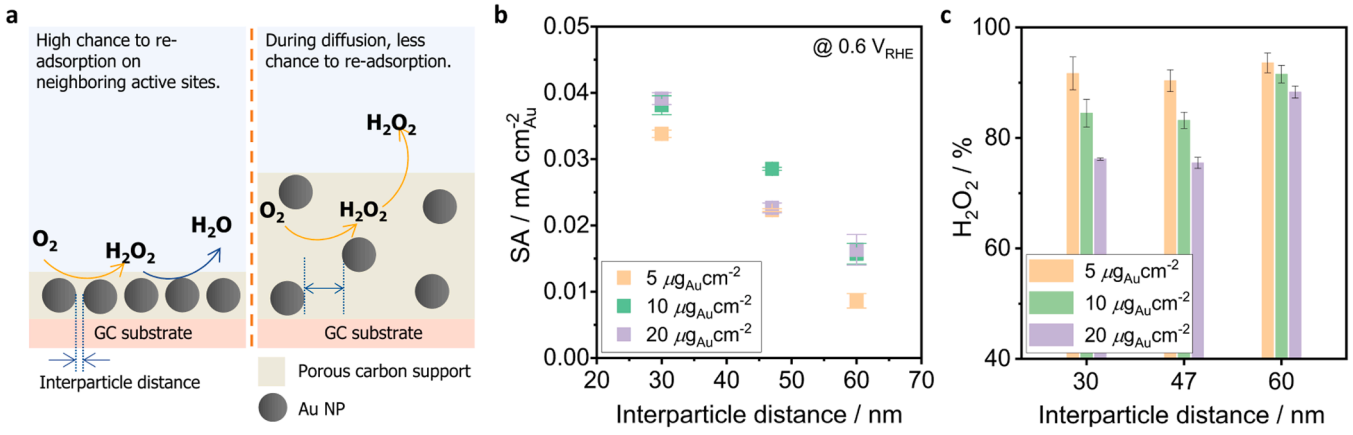

Fig. 4. (a) Schematic representation of the impact of interparticle distance on the H_2O_2 selectivity with particles embedded in a porous carbon support on a glassy carbon (GC) support. (b) Specific activity (SA) at 0.6 V_{RHE} for Au_3/C catalyst, with interparticle distances adjusted by Au to carbon ratio in the O_2-saturated 0.1 M $HClO_4$ electrolyte with a scan rate of 10 mV s^{-1} at 900 rpm. It also examines the impact of catalyst loading on these interparticle distances. (c) Averaged H_2O_2 selectivity, calculated across a potential range from 0.6 V to 0.1 V_{RHE}, as a function of interparticle distance.

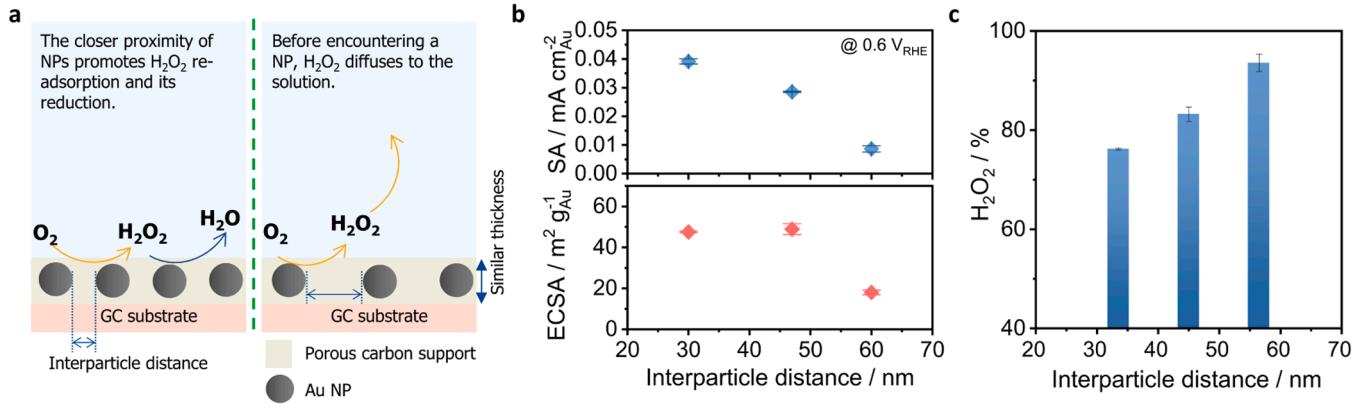

Fig. 5. (a) Schematic illustration of the impact of interparticle distance on the H_2O_2 selectivity within the similar catalyst layer thickness. (b) Specific activity (SA) at 0.6 V_{RHE} in the upper panel and ECSA of the Au_3/C catalysts in the lower panel with varying interparticle distances in O_2-saturated 0.1 M $HClO_4$ electrolyte, measured at a scan rate of 10 mV s^{-1} and rotation speed of 900 rpm. (c) Averaged H_2O_2 selectivity calculated from RRDE responses. The values for (b) and (c) were taken from Fig. 4b and Fig. 4c, respectively.

f. Figure S3) amplify the likelihood of H_2O_2 re-adsorption, driven by the stronger reductive potential, while denser nanoparticle populations in thicker films exacerbate this effect. This interplay between H_2O_2 desorption, diffusion, and re-adsorption underpins the observed selectivity trends. These findings underscore the pivotal role of both layer thickness and interparticle distance in catalytic performance, highlighting their critical importance in catalyst screening and optimization.

2.4. Impact of electrode thickness on H_2O_2 selectivity

To investigate the interplay between mass transport and H_2O_2 selectivity, we systematically adjusted the total catalyst loadings per geometric area of the electrode for each Au size. This adjustment allowed us to vary the thicknesses of the catalyst layer, as demonstrated in Fig. 6a. The estimated thickness of the catalyst layer, determined using the carbon density of 1.90 g cm^{-3} and an electrode area of 0.24 cm^2, resulted in values of 110, 210, and 420 nm for catalyst loadings of 25, 50, and 100 μg cm^{-2}, respectively. However, since this estimation assumes ideal packing, the actual layer thickness could be greater, considering the voids or spaces between primary carbon particles. To focus solely on the effect of catalyst layer thickness (i.e., with varying loading), we standardized the Au loading on the carbon support at 20 wt%. This ensured a consistent interparticle distance, also known as a crucial factor influencing catalytic performance. The SA remains almost constant for each Au particle size, independent of the catalyst loading, as shown in the upper panel of Fig. 6b. For further insights, the complete LSV curves are available in Figure S4 of the Supporting Information. Similarly, the trend for mass activity (MA) which reflects the reaction rate per unit mass of Au, exhibits minimal variability across different catalyst layer thicknesses. On the other hand, catalysts with higher activity levels exhibited more pronounced variations in H_2O_2 selectivity as a result of changes in catalyst loading. For Au_{10}/C, which necessitates higher overpotentials for ORR initiation, the selectivity remained relatively consistent across various loadings, as illustrated in Fig. 6c. In contrast, for Au_4/C, selectivity decreased from 93 % at 25 μg cm^{-2} to 77 % at 100 μg cm^{-2}. A similar trend was observed in Au_3/C, where H_2O_2 selectivity shifted from 92 % to 76 % as the catalyst layer thickness increased.

The results unequivocally demonstrate that the electrocatalytic performance and specificity of the $2e^-$ORR are significantly influenced by the catalyst loading on the disk electrode, which directly affects the thickness of the catalyst layer. Higher loading results in a thicker catalyst layer, potentially hindering the mass transport of both, the reactant and the intermediate H_2O_2 [24]. However, SA values demonstrating consistent 2-electron transfer oxygen reduction efficiency across different catalyst loadings imply that reactant transport through the catalyst layer does not limit oxygen reduction, even for Au particles in close proximity to the glassy carbon substrate [64]. Conversely, the produced H_2O_2 may be trapped within the pore system of the catalyst layer, facilitating its further reduction or chemical decomposition before

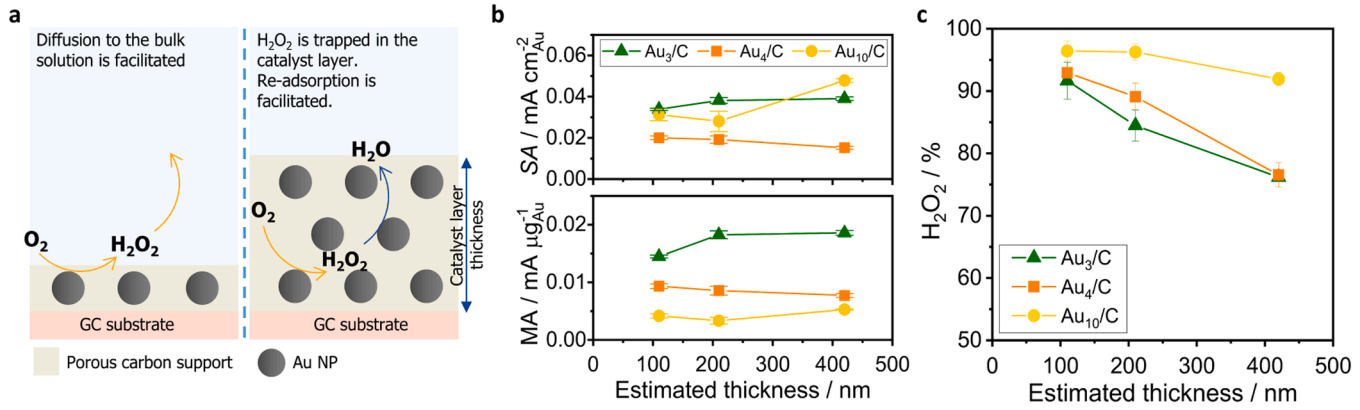

Fig. 6. (a) Schematic representation of the impact of catalyst loading on the ORR, showing how layer thickness affects re-adsorption and further reduction to water. (b) Specific activity (SA, upper panel) and mass activity (MA, lower panel) at 0.5 V_{RHE} for 20 wt% Au_x/C (x = 4 and 10) measured in O_2-saturated 0.1 M $HClO_4$ electrolyte at a scan rate of 10 mV s^{-1} and rotation speed of 900 rpm at various catalyst thicknesses. The SA and MA of Au_3/C were taken at 0.6 V_{RHE}. (c) Averaged H_2O_2 production selectivity from 0.5 to 0.1 V_{RHE} for Au_x/C (x = 4, and 10) and 0.6–0.1 V_{RHE} for Au_3/C.

diffusing into the bulk electrolyte. This process potentially reduces H_2O_2 selectivity by increasing catalyst loading, as shown in Fig. 6a and Fig. 6c.

In addition to trapping effects, the thickness of the catalyst layer also influences collection efficiency, which is determined by the ratio of the amount produced at the disk electrode to the amount detected at the ring electrode and largely depends on the dimensions of these electrodes [23,65]. Increased catalyst loading could lead to surface roughness due to cracking in the catalyst layer, changing the geometry of the RRDE and disrupting its hydrodynamic linearity [22,65]. Consequently, this affects collection efficiency and ultimately alters the selectivity of electrocatalysis. Conversely, insufficient catalyst loading may result in a substrate effect, where the observed activity predominantly originates from the substrate rather than the catalyst [66]. These findings emphasize the importance of considering catalyst loading, relating to catalyst layer thickness when determining optimal conditions for precise and equitable catalyst screening, especially in reactions that involve multiple pathways and require control over reaction selectivity.

Unless the ORR directly progresses to water through a dissociation pathway without involving H_2O_2 intermediates, systematic parameters and mesoscopic mass transport limitations, along with intrinsic parameters, will influence selectivity. These factors depend on the intermediates' residence time and their tendency for desorption and re-adsorption, which are strongly correlated with the affinity between oxygen/oxygen-containing intermediates and active sites. We demonstrated these effects using Au-based model catalyst, which binds weakly to oxygen/oxygen-containing intermediates. Therefore, the observed impact on ORR performance could be even more significant for catalysts with stronger oxygen affinity, such as platinum group metals (Pt, Pd, and Rh) [67,68] and non-noble metals (Co, Ni, and Fe) [24,25], according to the binding energy criteria. For ORR occurring on Fe- or Co-based catalysts, the reaction pathway can alter with variations in catalyst loading. A notable increase in H_2O_2 generation is observed as the catalyst loading decreases [24,25]. Furthermore, the produced H_2O_2 on these catalysts decomposes into reactive oxygen species, such as hydroxyl or hydroperoxyl radicals, during diffusion into the bulk electrolyte via Fenton/Fenton-like reaction [69]. This process can degrade the catalytic system or the membrane of polymer electrolyte membrane (PEM) fuel cells [70,71]. Translating our findings to practical H_2O_2-generating devices underscores the need to optimize interparticle distance and catalyst layer design in membrane electrode assemblies (MEAs) and gas diffusion electrodes (GDEs)—systems more reflective of industrial environments. Careful design can enhance mass transport, minimize H_2O_2 re-adsorption, and improve overall selectivity, thereby ensuring the long-term durability and efficiency of the H_2O_2 electrosynthesis process and supporting the scale-up of electrochemical devices. We emphasize the importance of integrating engineering solutions—such as tailored catalyst layer architectures and advanced support materials—to complement improvements in intrinsic catalytic activity and enable scalable, efficient H_2O_2 production. Specifically, in the context of H_2O_2-PEM electrolyzers, optimizing catalyst supports to facilitate the rapid transport of H_2O_2 away from the MEA, along with reactor designs that account for fluid dynamics to reduce intermediate residence time and limit re-adsorption, will be essential for advancing device performance.

3. Conclusion

Our study puts attention beyond traditional approaches of electrocatalytic evaluation by unveiling the critical interplay between intrinsic activity, systematic parameters, and mass transport limitations. We demonstrate that focusing solely on intrinsic catalyst properties provides an incomplete picture, as factors like interparticle distance, catalyst layer thickness, and surface area significantly influence selectivity in reactions with multiple pathways, like H_2O_2 production via ORR. The influence of these parameters on the selectivity depends strongly on the employed catalysts. This is evident from our findings with varying Au particle sizes supported on C, where the observed effects on catalytic performance could be even more significant for catalysts with stronger oxygen affinity, such as platinum group metals (Pt, Pd, and Rh), or in other electrocatalytic reactions. This work paves the way for optimizing H_2O_2 production through meticulous control of these parameters and provides a valuable framework for understanding and optimizing other multi-step electrocatalytic reactions. It highlights that previously observed changes in selectivity attributed solely to active site structure or electronic effects might be due, at least in part, to the interplay of these identified factors and that a collective investigation of all factors contributes to the overall performance. This broader understanding opens doors for the rational design of next-generation electrocatalysts with superior performance and selectivity.

CRediT authorship contribution statement

Ji Sik Choi: Writing – review & editing, Writing – original draft, Visualization, Validation, Methodology, Investigation, Formal analysis, Conceptualization. **Guilherme V. Fortunato:** Writing – review & editing, Writing – original draft, Validation, Supervision, Project administration, Formal analysis, Conceptualization. **Marko Malinovic:** Validation, Investigation, Formal analysis. **Ezra S. Koh:** Validation, Methodology, Investigation, Formal analysis. **Raquel Aymerich-Armengol:** Writing – review & editing, Validation, Methodology, Investigation, Formal analysis. **Christina Scheu:** Writing – review & editing, Validation, Project administration, Conceptualization. **Huize Wang:** Validation, Formal analysis, Conceptualization. **Andreas Hutzler:** Validation, Investigation, Formal analysis, Conceptualization. **Jan P. Hofmann:** Conceptualization, Funding acquisition, Project administration, Writing – review & editing. **Marcos R.V. Lanza:** Supervision, Project administration, Funding acquisition, Conceptualization. **Marc Ledendecker:** Writing – review & editing, Visualization, Supervision, Project administration, Funding acquisition, Conceptualization.

Declaration of Competing Interest

The authors declare that they have no known competing financial interests or personal relationships that could have appeared to influence the work reported in this paper.

Acknowledgment

J.S.C., M.M., E.S.K., and M.L. are grateful to the Federal Ministry of Education and Research (BMBF) for the financial support received in the framework of NanoMatFutur (SynKat, FK: 03XP0265). G.V.F. and M.R.V.L. acknowledge that this study was financed, in part, by the São Paulo Research Foundation (FAPESP), Brasil. Process Numbers #2019/04421-7, #2021/14194-8, and #2022/12895-1. They also thank the Brazilian National Council for Scientific and Technological Development (CNPq – grants#303943/2021-1) for additional support. H.W. and M.L. acknowledge financial support from the Helmholtz Networking and Initiative Fund. M.L. and J.P.H. gratefully acknowledge funding within the framework of Fe-Upgraded from the Deutsche Forschungsgemeinschaft (DFG, German Research Foundation) – Project-ID 443703006 – CRC 1487.

Declaration of Generative AI and AI-assisted technologies in the writing process

During the preparation of this work the author(s) used ChatGPT in order to improve the readability and language of the manuscript. After using this tool/service, the author(s) reviewed and edited the content as needed and take(s) full responsibility for the content of the published article.

Appendix A. Supporting information

Supplementary data associated with this article can be found in the online version at doi:10.1016/j.nanoen.2025.110811.

Data Availability

Data will be made available on request.

References

[1] J.M. Campos-Martin, G. Blanco-Brieva, J.L.G. Fierro, Hydrogen peroxide synthesis: an outlook beyond the anthraquinone process, Angew. Chem. Int. Ed. 45 (42) (2006) 6962–6984, https://doi.org/10.1002/anie.200503779.

[2] Chemanalyst. Decode the Future of Hydrogen Peroxide. ⟨https://www.chemanalyst.com/industry-report/hydrogen-peroxide-market-191⟩.

[3] S. Yang, A. Verdaguer-Casadevall, L. Arnarson, L. Silvioli, V. Čolić, R. Frydendal, J. Rossmeisl, I. Chorkendorff, I.E.L. Stephens, Toward the decentralized electrochemical production of H_2O_2: a focus on the catalysis, ACS Catal. 8 (5) (2018) 4064–4081, https://doi.org/10.1021/acscatal.8b00217.

[4] H.H. Heenen, H.S. Pillai, K. Reuter, V.J. Bukas, Exploring mesoscopic mass transport effects on electrocatalytic selectivity, Nat. Catal. (2024) 1–24, https://doi.org/10.1038/s41929-024-01177-6.

[5] H. Mistry, F. Behafarid, R. Reske, A.S. Varela, P. Strasser, B. Roldan Cuenya, Tuning catalytic selectivity at the mesoscale via interparticle interactions, ACS Catal. 6 (2) (2016) 1075–1080, https://doi.org/10.1021/acscatal.5b02202.

[6] H. Yang, S. Kumar, S. Zou, Electroreduction of O_2 on uniform arrays of Pt nanoparticles, J. Electroanal. Chem. 688 (2013) 180–188, https://doi.org/10.1016/j.jelechem.2012.08.030.

[7] A. Bonakdarpour, T.R. Dahn, R.T. Atanasoski, M.K. Debe, J.R. Dahn, H_2O_2 Release during oxygen reduction reaction on Pt nanoparticles, Electrochem. Solid-State Lett. 11 (11) (2008) 208–211, https://doi.org/10.1149/1.2978090.

[8] Y.E. Seidel, A. Schneider, Z. Jusys, B. Wickman, B. Kasemo, R.J. Behm, Mesoscopic mass transport effects in electrocatalytic processes, Faraday Discuss. 140 (2009) 167–184, https://doi.org/10.1039/B806437G.

[9] B. Zandkarimi, A.N. Alexandrova, Dynamics of subnanometer Pt clusters can break the scaling relationships in catalysis, J. Phys. Chem. Lett. 10 (3) (2019) 460–467, https://doi.org/10.1021/acs.jpclett.8b03680.

[10] J.S. Choi, S. Yoo, E.S. Koh, R. Aymerich-Armengol, C. Scheu, G.V. Fortunato, M.R. V. Lanza, Y.J. Hwang, M. Ledendecker, Unlocking the potential of sub-nanometer Pd catalysts for electrochemical hydrogen peroxide production, Adv. Mater. Interfaces 10 (36) (2023) 1–7, https://doi.org/10.1002/admi.202300647.

[11] S. Guerin, B.E. Hayden, D. Pletcher, M.E. Rendall, J.P. Suchsland, L.J. Williams, Combinatorial approach to the study of particle size effects in electrocatalysis: synthesis of supported gold nanoparticles, J. Comb. Chem. 8 (5) (2006) 791–798, https://doi.org/10.1021/cc060040k.

[12] E. Roduner, Size matters: why nanomaterials are different, Chem. Soc. Rev. 35 (7) (2006) 583–592, https://doi.org/10.1039/b502142c.

[13] M. Nesselberger, M. Roefzaad, R. Fayçal Hamou, P. Ulrich Biedermann, F. F. Schweinberger, S. Kunz, K. Schloegl, G.K.H. Wiberg, S. Ashton, U. Heiz, K.J. J. Mayrhofer, M. Arenz, The effect of particle proximity on the oxygen reduction rate of size-selected platinum clusters, Nat. Mater. 12 (10) (2013) 919–924, https://doi.org/10.1038/nmat3712.

[14] M. Shao, A. Peles, K. Shoemaker, Electrocatalysis on platinum nanoparticles: particle size effect on oxygen reduction reaction activity, Nano Lett. 11 (9) (2011) 3714–3719, https://doi.org/10.1021/nl2017459.

[15] W. Chen, S. Chen, Oxygen electroreduction catalyzed by gold nanoclusters: strong core size effects, Angew. Chem. 121 (24) (2009) 4450–4453, https://doi.org/10.1002/ange.200901185.

[16] W. Tang, H. Lin, A. Kleiman-shwarsctein, G.D. Stucky, E.W. Mcfarland, Size-dependent activity of gold nanoparticles for oxygen electroreduction in alkaline electrolyte, J. Phys. Chem. C. 112 (2008) 10515–10519.

[17] J. Speder, L. Altmann, M. Bäumer, J.J.K. Kirkensgaard, K. Mortensen, M. Arenz, The particle proximity effect: from model to high surface area fuel cell catalysts, RSC Adv. 4 (29) (2014) 14971–14978, https://doi.org/10.1039/c4ra00261j.

[18] J. Huang, J. Zhang, M.H. Eikerling, Particle proximity effect in nanoparticle electrocatalysis: surface charging and electrostatic interactions, J. Phys. Chem. C 121 (9) (2017) 4806–4815, https://doi.org/10.1021/acs.jpcc.6b10842.

[19] M. Inaba, A. Zana, J. Quinson, F. Bizzotto, C. Dosche, A. Dworzak, M. Oezaslan, S. B. Simonsen, L.T. Kuhn, M. Arenz, The oxygen reduction reaction on Pt: why particle size and interparticle distance matter, ACS Catal. 11 (12) (2021) 7144–7153, https://doi.org/10.1021/acscatal.1c00652.

[20] J. Cheng, C. Lyu, G. Dong, Y. Liu, Y. Hu, B. Han, D. Geng, D. Zhao, The underlying mechanism trade-off between particle proximity effect and low-Pt loading for oxygen reduction and methanol oxidation reaction activity, Electrochim. Acta 454 (April) (2023) 142364, https://doi.org/10.1016/j.electacta.2023.142364.

[21] G.V. Fortunato, E. Pizzutilo, A.M. Mingers, O. Kasian, S. Cherevko, E.S.F. Cardoso, K.J.J. Mayrhofer, G. Maia, M. Ledendecker, Impact of palladium loading and interparticle distance on the selectivity for the oxygen reduction reaction toward hydrogen peroxide, J. Phys. Chem. C. 122 (28) (2018) 15878–15885, https://doi.org/10.1021/acs.jpcc.8b04262.

[22] U.A. Paulus, T.J. Schmidt, H.A. Gasteiger, R.J. Behm, Oxygen reduction on a high-surface area Pt/Vulcan carbon catalyst: a thin-film rotating ring-disk electrode study, J. Electroanal. Chem. 495 (2) (2001) 134–145, https://doi.org/10.1016/S0022-0728(00)00407-1.

[23] J.S. Lim, J. Kim, K.S. Lee, Y.J. Sa, S.H. Joo, Impact of catalyst loading of atomically dispersed transition metal catalysts on H_2O_2 electrosynthesis selectivity, Electrochim. Acta 444 (2023) 142031, https://doi.org/10.1016/j.electacta.2023.142031.

[24] A. Bonakdarpour, M. Lefevre, R. Yang, F. Jaouen, T. Dahn, J.-P. Dodelet, J.R. Dahn, Impact of loading in RRDE experiments on Fe–N–C catalysts: two- or four-electron oxygen reduction, Electrochem. Solid-State Lett. 11 (6) (2008) B105, https://doi.org/10.1149/1.2904768.

[25] A. Muthukrishnan, Y. Nabae, T. Okajima, T. Ohsaka, Kinetic approach to investigate the mechanistic pathways of oxygen reduction reaction on Fe-containing N-doped carbon catalysts, ACS Catal. 5 (9) (2015) 5194–5202, https://doi.org/10.1021/acscatal.5b00397.

[26] P.J.M. Cordeiro-Junior, M.S. Kronka, L.A. Goulart, N.C. Veríssimo, L.H. Mascaro, M.C. dos Santos, R. Bertazzoli, M.R. de V. Lanza, Catalysis of oxygen reduction reaction for H_2O_2 electrogeneration: the impact of different conductive carbon matrices and their physicochemical properties, J. Catal. 392 (2020) 56–68, https://doi.org/10.1016/j.jcat.2020.09.020.

[27] E. Sedano Varo, R. Egeberg Tankard, J. Kryger-Baggesen, J. Jinschek, S. Helveg, I. Chorkendorff, C.D. Damsgaard, J. Kibsgaard, Gold nanoparticles for CO_2 electroreduction: an optimum defined by size and shape, J. Am. Chem. Soc. 146 (3) (2024) 2015–2023, https://doi.org/10.1021/jacs.3c10610.

[28] Y. Tang, Z. Zhang, M. Lu, B. Chen, W. Fu, J. Gan, G. Qian, X. Duan, X. Zhou, Site-dependent activity and selectivity of H_2O_2 formation from H_2 and O_2 over Au-based catalysts, Ind. Eng. Chem. Res (2019), https://doi.org/10.1021/acs.iecr.9b01459.

[29] B.R. Cuenya, S.H. Baeck, T.F. Jaramillo, E.W. McFarland, Size- and support-dependent electronic and catalytic properties of Au^0/Au^{3+} nanoparticles synthesized from block copolymer micelles, J. Am. Chem. Soc. 125 (42) (2003) 12928–12934, https://doi.org/10.1021/ja036468u.

[30] S. Peters, S. Peredkov, M. Neeb, W. Eberhardt, M. Al-Hada, Size-dependent XPS spectra of small supported Au-clusters, Surf. Sci. 608 (2013) 129–134, https://doi.org/10.1016/j.susc.2012.09.024.

[31] Y. Sun, Y. Cao, L. Wang, X. Mu, Q. Zhao, R. Si, X. Zhu, S. Chen, B. Zhang, D. Chen, Y. Wan, Gold catalysts containing interstitial carbon atoms boost hydrogenation activity, Nat. Commun. 11 (1) (2020) 1–9, https://doi.org/10.1038/s41467-020-18322-x.

[32] P. Chauhan, K. Hiekel, J.S. Diercks, J. Herranz, V.A. Saveleva, P. Khavlyuk, A. Eychmüller, T.J. Schmidt, Electrochemical surface area quantification, CO_2 reduction performance, and stability studies of unsupported three-dimensional Au aerogels versus carbon-supported Au nanoparticles, ACS Mater. Au (2021), https://doi.org/10.1021/acsmaterialsau.1c00067.

[33] S. Guerin, B.E. Hayden, C.E. Lee, C. Mormiche, J.R. Owen, A.E. Russell, B. Theobald, D. Thompsett, Combinatorial electrochemical screening of fuel cell electrocatalysts, J. Comb. Chem. 6 (1) (2004) 149–158, https://doi.org/10.1021/cc030113p.

[34] J.T. Steven, V.B. Golovko, B. Johannessen, A.T. Marshall, Electrochemical stability of carbon-supported gold nanoparticles in acidic electrolyte during cyclic voltammetry, Electrochim. Acta 187 (2016) 593–604, https://doi.org/10.1016/j.electacta.2015.11.096.

[35] L. Tang, X. Meng, D. Deng, X. Bao, Confinement catalysis with 2D materials for energy conversion, Adv. Mater. 31 (50) (2019), https://doi.org/10.1002/adma.201901996.

[36] Y. Iizuka, T. Tode, T. Takao, K.I. Yatsu, T. Takeuchi, S. Tsubota, M. Haruta, A kinetic and adsorption study of CO oxidation over unsupported fine gold powder and over gold supported on titanium dioxide, J. Catal. 187 (1) (1999) 50–58, https://doi.org/10.1006/jcat.1999.2604.

[37] M.M. Montemore, M.A. Van Spronsen, R.J. Madix, C.M. Friend, O_2 activation by metal surfaces: implications for bonding and reactivity on heterogeneous catalysts, Chem. Rev. 118 (5) (2018) 2816–2862, https://doi.org/10.1021/acs.chemrev.7b00217.

[38] B.C. Han, C.R. Miranda, G. Ceder, Effect of particle size and surface structure on adsorption of O and OH on platinum nanoparticles: a first-principles study, Phys. Rev. B Condens Matter Mater. Phys. 77 (7) (2008) 1–9, https://doi.org/10.1103/PhysRevB.77.075410.

[39] J. Zhang, H.Bin Yang, D. Zhou, B. Liu, Adsorption energy in oxygen electrocatalysis, Chem. Rev. 122 (23) (2022) 17028–17072, https://doi.org/10.1021/acs.chemrev.1c01003.

[40] W. Zhou, M. Li, O.L. Ding, S.H. Chan, L. Zhang, Y. Xue, Pd particle size effects on oxygen electrochemical reduction, Int J. Hydrog. Energy 39 (12) (2014) 6433–6442, https://doi.org/10.1016/j.ijhydene.2014.01.197.

[41] K. Kinoshita, Particle size effects for oxygen reduction on highly dispersed platinum in acid electrolytes, J. Electrochem Soc. 137 (3) (1990) 845–848, https://doi.org/10.1149/1.2086566.

[42] J.A. Van Bokhoven, J.T. Miller, D electron density and reactivity of the D band as a function of particle size in supported gold catalysts, J. Phys. Chem. C. 111 (26) (2007) 9245–9249, https://doi.org/10.1021/jp070755t.

[43] J. Greeley, J. Rossmeisl, A. Hellman, J.K. Nørskov, Theoretical trends in particle size effects for the oxygen reduction reaction, Z. fur Phys. Chem. 221 (9–10) (2007) 1209–1220, https://doi.org/10.1524/zpch.2007.221.9-10.1209.

[44] R.R. Adžić, S. Strbac, N. Anastasijević, Electrocatalysis of oxygen on single crystal gold electrodes, Mater. Chem. Phys. 22 (3–4) (1989) 349–375, https://doi.org/10.1016/0254-0584(89)90005-9.

[45] M. Alvarez-Rizatti, K. Jüttner, Electrocatalysis of oxygen reduction by UPD of lead on gold single-crystal surfaces, J. Electro Chem. Interfacial Electrochem 144 (1–2) (1983) 351–363, https://doi.org/10.1016/S0022-0728(83)80166-1.
[46] A. Prieto, J. Hernández, E. Herrero, J.M. Feliu, The role of anions in oxygen reduction in neutral and basic media on gold single-crystal electrodes, J. Solid State Electrochem. 7 (9) (2003) 599–606, https://doi.org/10.1007/s10008-003-0362-3.
[47] S. Štrbac, N.A. Anastasijević, R.R. Adžić, Oxygen reduction on Au(111) and vicinal Au(332) faces: a rotating disc and disc-ring study, Electrochim. Acta 39 (7) (1994) 983–990, https://doi.org/10.1016/0013-4686(94)85116-6.
[48] S.R. Kelly, C. Kirk, K. Chan, J.K. Nørskov, Electric Field Effects in Oxygen Reduction Kinetics: Rationalizing Ph Dependence at the Pt(111), Au(111), and Au (100) Electrodes. AIChE Annual Meeting, Conference Proceedings, American Institute of Chemical Engineers, 2020, pp. 14581–14591, https://doi.org/10.1021/acs.jpcc.0c02127. Vol. 2020-November.
[49] R.R. Adžić, A.V. Tripković, N.M. Marković, Structural effects in electrocatalysis. oxidation of formic acid and oxygen reduction on single-crystal electrodes and the effects of foreign metal adatoms, J. Electroanal. Chem. 150 (1–2) (1983) 79–88, https://doi.org/10.1016/S0022-0728(83)80192-2.
[50] A.M. Gómez-Marín, A. Boronat, J.M. Feliu, Electrocatalytic oxidation and reduction of H_2O_2 on Au single crystals, Russ. J. Electrochem. 53 (9) (2017) 1029–1041, https://doi.org/10.1134/S1023193517090063.
[51] Z. Jusys, R.J. Behm, The effect of anions and PH on the activity and selectivity of an annealed polycrystalline Au film electrode in the oxygen reduction reaction-revisited, ChemPhysChem 20 (24) (2019) 3276–3288, https://doi.org/10.1002/cphc.201900960.
[52] E. Diesen, A.M. Dudzinski, K. Reuter, V.J. Bukas, On the origin of electrocatalytic selectivity during the oxygen reduction reaction on Au(111), Chemrxiv (2024), https://doi.org/10.26434/chemrxiv-2024-7jj5n.
[53] A.M. Dudzinski, E. Diesen, H.H. Heenen, V.J. Bukas, K. Reuter, First step of the oxygen reduction reaction on Au(111): a computational study of O_2 adsorption at the electrified metal/water interface, ACS Catal. 13 (18) (2023) 12074–12081, https://doi.org/10.1021/acscatal.3c02129.
[54] Y. Yang, C. Dai, A. Fisher, Y. Shen, D. Cheng, A full understanding of oxygen reduction reaction mechanism on Au(1 1 1) surface, J. Phys. Condens. Matter 29 (36) (2017), https://doi.org/10.1088/1361-648X/aa7db6.
[55] R.B. Rankin, J. Greeley, Trends in selective hydrogen peroxide production on transition metal surfaces from first principles, ACS Catal. 2 (12) (2012) 2664–2672, https://doi.org/10.1021/cs3003337.
[56] S. Proch, K. Kodama, M. Inaba, K. Oishi, N. Takahashi, Y. Morimoto, The "particle proximity effect" in three dimensions: a case study on vulcan XC 72R, Electrocatalysis 7 (3) (2016) 249–261, https://doi.org/10.1007/s12678-016-0302-5.
[57] E. Antolini, Structural parameters of supported fuel cell catalysts: the effect of particle size, inter-particle distance and metal loading on catalytic activity and fuel cell performance, Appl. Catal. B 181 (2016) 298–313, https://doi.org/10.1016/j.apcatb.2015.08.007.
[58] S. Taylor, E. Fabbri, P. Levecque, T.J. Schmidt, O. Conrad, The effect of platinum loading and surface morphology on oxygen reduction activity, Electrocatalysis 7 (4) (2016) 287–296, https://doi.org/10.1007/s12678-016-0304-3.
[59] G.V. Fortunato, M.S. Kronka, A.J. dos Santos, M. Ledendecker, M.R.V. Lanza, Low Pd loadings onto Printex L6: synthesis, characterization and performance towards H_2O_2 generation for electrochemical water treatment technologies, Chemosphere 259 (2020) 127523, https://doi.org/10.1016/j.chemosphere.2020.127523.
[60] X. Li, A.A. Gewirth, Peroxide electroreduction on Bi-modified Au surfaces: vibrational spectroscopy and density functional calculations, J. Am. Chem. Soc. 125 (23) (2003) 7086–7099, https://doi.org/10.1021/ja034125q.
[61] X. Li, A.A. Gewirth, Oxygen electroreduction through a superoxide intermediate on Bi-modified Au surfaces, J. Am. Chem. Soc. 127 (14) (2005) 5252–5260, https://doi.org/10.1021/ja043170a.
[62] N. Ohta, K. Nomura, I. Yagi, Adsorption and electroreduction of oxygen on gold in acidic media: in situ spectroscopic identification of adsorbed molecular oxygen and hydrogen superoxide, J. Phys. Chem. C. 116 (27) (2012) 14390–14400, https://doi.org/10.1021/jp302857q.
[63] D. Mei, Z.Da He, Y.L. Zheng, D.C. Jiang, Y.X. Chen, Mechanistic and kinetic implications on the ORR on a Au(100) electrode: PH, temperature and H-D kinetic isotope effects, Phys. Chem. Chem. Phys. 16 (27) (2014) 13762–13773, https://doi.org/10.1039/c4cp00257a.
[64] H. Erikson, G. Jürmann, A. Sarapuu, R.J. Potter, K. Tammeveski, Electroreduction of oxygen on carbon-supported gold catalysts, Electrochim. Acta 54 (28) (2009) 7483–7489, https://doi.org/10.1016/j.electacta.2009.08.001.
[65] R. Zhou, Y. Zheng, M. Jaroniec, S.Z. Qiao, Determination of the electron transfer number for the oxygen reduction reaction: from theory to experiment, ACS Catal. 6 (7) (2016) 4720–4728, https://doi.org/10.1021/acscatal.6b01581.
[66] J.S. Lim, Y.J. Sa, S.H. Joo, Catalyst design, measurement guidelines, and device integration for H_2O_2 electrosynthesis from oxygen reduction, Cell Rep. Phys. Sci. 3 (8) (2022) 100987, https://doi.org/10.1016/j.xcrp.2022.100987.
[67] E.J. Biddinger, D. von Deak, D. Singh, H. Marsh, B. Tan, D.S. Knapke, U.S. Ozkan, Examination of catalyst loading effects on the selectivity of CNx and Pt/VC ORR catalysts using RRDE, J. Electrochem Soc. 158 (4) (2011) B402, https://doi.org/10.1149/1.3552944.
[68] K. Ke, T. Hatanaka, Y. Morimoto, Reconsideration of the quantitative characterization of the reaction intermediate on electrocatalysts by a rotating ring-disk electrode: the intrinsic yield of H_2O_2 on Pt/C, Electro Acta 56 (5) (2011) 2098–2104, https://doi.org/10.1016/j.electacta.2010.11.086.
[69] J.S. Choi, G.V. Fortunato, D.C. Jung, J.C. Lourenço, M.R.V. Lanza, M. Ledendecker, Catalyst durability in electrocatalytic H_2O_2 production: key factors and challenges, Nanoscale Horiz. (2024), https://doi.org/10.1039/D4NH00109E.
[70] K. Kumar, L. Dubau, M. Mermoux, J. Li, A. Zitolo, J. Nelayah, F. Jaouen, F. Maillard, On the influence of oxygen on the degradation of Fe-N-C catalysts, Angew. Chem. 132 (8) (2020) 3261–3269, https://doi.org/10.1002/ange.201912451.
[71] X. Xie, C. He, B. Li, Y. He, D.A. Cullen, E.C. Wegener, A.J. Kropf, U. Martinez, Y. Cheng, M.H. Engelhard, M.E. Bowden, M. Song, T. Lemmon, X.S. Li, Z. Nie, J. Liu, D.J. Myers, P. Zelenay, G. Wang, G. Wu, V. Ramani, Y. Shao, Performance enhancement and degradation mechanism identification of a single-atom Co–N–C CAtalyst for Proton Exchange Membrane Fuel Cells, Nat. Catal. 3 (12) (2020) 1044–1054, https://doi.org/10.1038/s41929-020-00546-1.

Ji Sik Choi earned a B.Sc. in Engineering from Kyonggi University in 2008 and an M.Sc. in Clean Energy and Chemical Engineering from the Korea University of Science and Technology (UST-KIST) in 2012. Since 2021, she has been conducting her Ph.D. research at the Technical University of Darmstadt, focusing on the design of stable Pd-based single-atom catalysts for efficient electrocatalytic H_2O_2 production.

Guilherme V. Fortunato earned his Ph.D. in Chemistry/Electrochemistry in 2019 from the Federal University of Mato Grosso do Sul, with a research stay at the Max Planck Institute for Iron Research. He pursued postdoctoral research as a FAPESP fellow at the University of São Paulo and the Technical University of Darmstadt. Since 2023, he has been a senior postdoctoral researcher and sub-group leader at the Technical University of Munich. His research focuses on developing functional nanomaterials for electrochemical energy and environmental applications, with an emphasis on integrating thermo- and electrocatalysis.

Marko Malinovic earned his B.Sc. in Materials Engineering (2016) and M.Sc. in Materials Science and Engineering (2017) from the Faculty of Technology Novi Sad. Since 2021, he has been pursuing his Ph.D. at the Technical University of Darmstadt. His research focuses on developing iridium-based electrocatalysts for the oxygen evolution reaction in acidic media.

Ezra S. Koh earned his B.Eng. in Chemical Technology (2016) from Darmstadt University of Applied Sciences and his M.Sc. in Chemistry (2017) from the Technical University of Darmstadt. Since 2020, he has been pursuing his Ph.D. at the Technical University of Darmstadt, focusing on designing stable copper nanocatalysts for the electrochemical CO_2 reduction reaction.

Raquel Aymerich-Armengol earned her Ph.D. in Chemistry of Materials in 2023 at the Max Planck Institute for Iron Research, with a research stay at Kangwon National University. She is currently a postdoctoral researcher at the Center for Visualizing Catalytic Processes of the Technical University of Denmark. Her research focuses on understanding synthesis-structure-property relationships of nanomaterials for electrochemical applications using in-situ, identical location, and ex-situ electron microscopy techniques.

Prof. Christina Scheu is a full professor in the field of Materials Analytics at RWTH Aachen University and leads an independent research group on Nanoanalytics and Interfaces at the Max Planck Institute for Sustainable Materials in Düsseldorf, Germany. She is a physicist by training and obtained her Ph.D. in materials science. Prof. Scheu is an expert in unravelling the atomic arrangement and local composition of defects in materials using advanced ex-situ and in-situ scanning transmission electron microscopy, with a strong focus on materials for renewable energy applications.

Huize Wang earned his M.Sc. in Chemistry in 2020 from Humboldt University of Berlin and his Ph.D. in Chemistry in 2023 from the Max Planck Institute of Colloids and Interfaces (Humboldt University of Berlin). Since 2023, he has been a senior postdoctoral researcher and sub-group leader at the Helmholtz Institute Erlangen-Nürnberg. His research focuses on developing novel synthesis approaches for nanostructured catalysts in electrochemical energy and environmental applications.

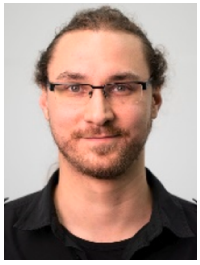

Andreas Hutzler studied electrical engineering with a focus on semiconductor technology, photonics, and medical electronics at Friedrich-Alexander-Universität Erlangen-Nürnberg. During his doctorate, he developed new liquid cell architectures and applied those in the field of material's research to study growth and degradation mechanisms of nanostructures using liquid-phase transmission electron microscopy (LP-TEM). Since 2018, he works on understanding and modeling beam damage in LP-TEM. In 2021, he joined HIERN as a team leader and head of TEM lab. Since then, his focus has been extended towards applying LP-TEM for studying degradation mechanisms of energy materials utilized in electrocatalysis for hydrogen production.

Prof. Jan Philipp Hofmann is a chemist and full professor of Surface Science at the Technical University of Darmstadt, Germany since 2020. He received his academic education and Dr. rer. nat. from Justus-Liebig-University Giessen, Germany followed by a postdoctoral stay at the Debye Institute of Nanomaterials Science at Utrecht University, The Netherlands. Between 2013 and 2020, he has been assistant professor for Solar Fuels Catalysis and Inorganic Materials Chemistry at Eindhoven University of Technology, The Netherlands. His current research focuses on the investigation of interface chemistry, energetics and dynamics of renewable energy conversion and storage devices and materials using surface science and in-situ/operando approaches.

Prof. Marcos R.V. Lanza earned his Ph.D. in Mechanical Engineering in 2001 from the University of Campinas (UNICAMP), Brazil. He was a visiting professor at INRS-EMT, Canada (2019), and the University of Castilla-La Mancha, Spain (2023). He is an Associate Professor at the Institute of Chemistry of São Carlos at the University of São Paulo and leads the Electrochemical and Environmental Processes Group (GPEA). His research focuses on environmental and applied electrochemistry, including electrocatalysts, gas diffusion electrodes, electrochemical hydrogen peroxide generation, wastewater treatment, and advanced electrochemical oxidation processes (AEOP).

Prof. Marc Ledendecker received his Ph.D. in Materials Science in 2016 from the Max Planck Institute of Colloids and Interfaces, with a research stay at the Weizmann Institute of Science. He continued as a postdoc and project coordinator at the Max Planck Institute for Iron Research and the University of California, Berkeley. He began his independent career at the Technical University of Darmstadt and became a tenure-track professor at the Technical University of Munich in 2022. His research focuses on nanoscale material synthesis and electrocatalysis, emphasizing sustainable energy conversion and catalyst stability.